Published in final edited form as:
Biomacromolecules. 2008 January ; 9(1): 199–207. doi:10.1021/bm700973t.

An in-situ Study of Collagen Self-Assembly Processes

Sarah Köster[1,2,a], **Heather M. Evans**[1], **Joyce Y. Wong**[2], and **Thomas Pfohl**[1,*]

1 *Max Planck Institute for Dynamics and Self-Organization, Bunsenstraße 10, 37073 Göttingen, Germany*

2 *Department of Biomedical Engineering, Boston University, 44 Cummington Street, Boston, MA 02215, USA*

Abstract

We present *in situ* studies on the self-assembly and dynamic evolution of collagen gels from semi-dilute solutions in a microfluidic device. Collagen fibrils not only reinforce the mechanical properties of bone and tissues, but they also influence cellular motility and morphology. We access the initial steps of the hierarchical self-assembly of collagen fibrils and networks by using hydrodynamic focusing to form oriented fibers. The accurate description of the conditions within the microchannel requires a numerical expression for the pH in the device, as well as a modified mathematical description of the viscosity, which increases nearly 300-fold as collagen fibrils form around neutral pH. Finite element modeling profiles overlay impressively with crossed polarized microscopy images of the birefringent fibrils in the channel. Real-time X-ray microdiffraction measurements in flow indicate an enhanced supramolecular packing having a unit spacing commensurate with that of a pentameric collagen subunits. These results have significant implications for the field of biomedicine, wherein new aligned, cellularly active, and mechanically strengthened materials continue to be in demand. However, this work is also remarkable from a more fundamental, biophysical point of view, since the underlying concepts may be generalized to a large pool of systems.

Keywords

Collagen; self-assembly; hierarchical structures; microfluidics; polarization microscopy; X-ray microdiffraction

Introduction

Collagens are a family of fibrous proteins which are found in all multicellular organisms. They are the major component of bone and skin and represent about 25% of the total protein mass in animals. More than 20 different types have been identified and classified primarily according to their physiological structure. Here we focus on collagen I, which represents 90% of the total body collagen and belongs to the category of fibril-forming proteins. The macroscale structure and organization of collagen I fibrils are key contributors to the mechanical properties of soft tissue, bone, tendon, and ligaments. Furthermore, the organization of collagen on the microscale profoundly influences cell morphology, migration, proliferation and gene expression.[1] In the extracellular space, collagen molecules hierarchically self-assemble at the nano-, micro-, and macroscales into many different structures that are suited to their physiological function. While the linear periodicity of collagen fibrils is rather easy to detect by electron microscopy,[2] much more effort needs to be devoted to the investigation of lateral packing. In particular, the organization of the critical subunits remains unresolved[3] despite the existence of theoretical models and some X-ray data. Interestingly, the formation of a 4 nm

*Corresponding author: tel: +49-551-5176-240, fax: +49-551-5176-202.
[a]Current address: Dept. of Physics/SEAS, Harvard University, 40 Oxford St., Cambridge, MA 02138, USA

microfibril as the critical subunit of collagen self-assembly has been observed in isolated *in vivo* systems[4,5] as well as in *in vitro* systems.[6] This ordering is considered to be the next hierarchical step from the fundamental triple helix of collagen, which itself has a pitch of 10 nm and diameter of 1.5 nm. Until now, there has not been a study using X-ray diffraction to elucidate the molecular packing of *in vitro* assembled collagen.

With respect to mechanical properties, the alignment of collagen fibrils plays a clear role: by aligning in the direction of highest strain, the collagen fibrils act as reinforcement to the tissue structure.[7] Aligned collagen fibers can also guide cell migration through contact guidance.[8] To this end, much research effort has been devoted to preparing aligned collagen networks through the use of intense magnetic[9] or electric fields, cell-generated traction forces[10] hydrodynamic flow,[11] and dip-pen nanolithography.[12] However, most of these methods lack microscale control of the self-assembly process, and none are amenable to dynamic investigations of the self-assembly process. At the same time, artificial 2D and 3D matrices are needed for the study of cell behavior in controlled microenvironment and for tissue engineering. We are thus particularly interested in controlling structural properties, such as the degree of alignment, while concurrently investigating the dynamics of the assembly process *in situ*.[13,14,15] To achieve this goal we use microfluidic tools to create defined flow fields and pH gradients, both of which together lead to the formation of collagen substructures. Microfluidics, in combination with light microscopy and X-ray microdiffraction, is a powerful tool for the investigation of a variety of biophysical scenarios, including the creation of new liquid-crystalline phases and oriented materials. The incorporation of appropriate modeling tools with these experimental techniques leads to new insights which can then be applied to the development of new biologically active assemblies with applications in the material and biological sciences.[13,14]

Experimental Methods

A 10 mg/mL solution of collagen I (from calf skin, USB Corporation, Cleveland, OH, USA) in 0.075 M acetic acid (AcH, ~ pH 3) is used without any further purification or dilution steps. The pH of the AcH solution is slightly increased to 3.7 upon dissolution of collagen. However, we disregard this buffering effect here in order to simplify the description of the system. Assumedly, the difference in the absolute value of the pH only weakly affects the pH conditions discussed here. The collagen solution as obtained from the manufacturer contains trimers of collagen peptide chains (MW ~ 285 kDa). These triple helical collagen molecules are stable at acidic pH and assemble into fibrils at neutral to basic pH often referred to as fibrillogenesis[16] or gelation.[6]

The microfluidic flow chambers for microscopy measurements are fabricated by soft lithography.[17,18] SU-8 50 negative photo resist (Micro Resist Technology GmbH, Berlin, Germany) is spin coated onto silicon wafers to a layer thickness 35 μm and patterned through a lithography transparency (JD-Photo-Tools Ltd., Oldham, UK). The wafers with the developed structures are treated with heptafluoropropyl-trimethylsilane (97%, Sigma), Sylgard 184 PDMS (Dow Corning GmbH, Wiesbaden, Germany) is mixed with the crosslinker (ratio 10:1), degassed thoroughly, poured onto the three-dimensional microstructures, and cured. The PDMS replicas are peeled off the wafer, bonded to cover slips, and used for the experiments.

The experiments described here involve the dynamic observation of collagen fibril formation and alignment. To be able to apply a controlled flow and stress to the biopolymers while establishing a stable pH gradient, a hydrodynamical focusing device is used. [13,19] A schematic representation of the device is shown in figure 1a–b.

The device consists of two perpendicularly crossed channels[18,20] which have a depth of 35 fm and a width of 100 μm. The microfluidic device is connected via polyethylene (Becton Dickinson & Co., Sparks, MD, USA) and Teflon (NovoDirect, Kehl, Germany) tubing to custom-made syringe pumps, which in turn are driven by programs written in LabVIEW (National Instruments Corporation, Austin, TX, USA). Collagen solution is injected into the main channel. Depending on the experimental requirements, different concentrations of NaOH (0.075 – 0.5 M, pH 13 – 14) are injected into the side channels. The NaOH-solution can be further diluted with water using T-valves. The flow into the side channels hydrodynamically focuses the collagen stream. The fluid velocity in the main channel (0.84 – 8.1 mm/s) is slower than the side channels (1.26 – 40.5 mm/s). In this configuration, the pH of the collagen solution gradually increases along the length of the outlet channel resulting from diffusive mixing with the NaOH.[13,21] Unless otherwise stated, the chemicals are from Sigma.

Polarization micrographs were obtained with an Olympus BX61 microscope equiped with crossed polarizers, a 10x objective, a halogen illumination system, and a PCO (Kehlheim, Germany) SensiCamQE camera.

For the X-ray experiments, a specially developed flow chamber is used[14,20] as shown in figure 1d. The cross geometry of width 150 μm is spark eroded into a stainless steel plate 300 μm. Both sides of the steel plate are covered with self-adhesive Kapton polyimide foil (Dr. D. Müller GmbH, Ahlhorn, Germany). To complete the device, holes are punched into one of the Kapton foils and tubing is connected to the flow chamber using homemade clips.

The small angle X-ray microdiffraction experiments are conducted at the beam-line ID10B of the European Synchrotron Radiation Facility (ESRF, Grenoble, France). The ID10B beam-line is a multi-purpose, high-brilliance undulator beam-line for high resolution X-ray scattering and surface diffraction on solids and liquids.[22] The microdiffraction set-up is sketched in figure 1c. The microfluidic device is mounted onto a goniometer and the X-ray beam is adjusted by using focusing optics mounted onto a secondary stage for optical elements. Beryllium compound refractive lenses (CRL),[23,24] are used to focus the X-ray beam down to a spot of 20 μm. The CRL have a focal distance of 1.30 m. For detection we use a CCD camera with fluorescent screen. The resultant 2D images of the diffraction patterns cover a q-range from 0.2 to 2.5 nm^{-1}. The smectic A layer spacing of the liquid crystal 8CB (4′-n-octyl-4-cyanobiphenyl, Sigma) serves as calibration. The exposure time of a single image is 30 s. Additional in-house ‘bulk experiments’ in quartz capillaries are performed using a Bruker (Karlsruhe, Germany) AXS Nanostar. A q-range from 0.1 to 8.0 nm^{-1} can be achieved. The setup includes a rotating anode X-ray source for Cu-K radiation 1.54 Å at a generator power of 4.05 kW and a virtually noise-free, real-time 2D Hi-Star detector with photon counting ability.[15]

Results and Discussion

In figure 1b, a schematic representation of the flow conditions in the microchannels is shown. Apart from the flow rates, both the diffusion constants and viscosities of the reagents and solutions in the microfluidic device determine the observable hydrodynamic and diffusive phenomena. Particularly, if the solutions in the main and side inlet channels have different pH values, a stable pH-gradient is established by diffusive mixing of the solutions. This gradient enables us to perform non-equilibrium measurements in continuous flow. The sudden increase in overall flow rate at the confluence of all three inlet streams in the center of the crossed channels additionally induces an elongational flow, which aligns and stretches the biomolecules. This allows for controlled manipulation of individual macromolecules and investigation of the influence of external stress on molecular dynamics and relaxation phenomena.[18] Furthermore, the extension and alignment of fibrous molecules improves the

formation of liquid crystalline phases.[14] This facilitates the investigation by polarization microscopy and X-ray diffraction. The flows in the microfluidic devices are governed by laminar flow (Reynolds number $Re < 1.6$) and all fluid dynamical phenomena are stationary. Therefore, we can observe different stages of the interaction between the reagents in the center and side streams at different positions within the outlet channel. Altogether, the hydrodynamic focusing and diffusive mixing device represents a very well-suited method to prepare aligned collagen gels in a controlled manner. The collagen self-assembles in a stable pH-gradient and enables us to observe this process *in situ* by means of different characterization methods.

The experimental results are elaborated as follows: we first discuss the influence of viscosity of a low pH collagen solution on fluid dynamics in the microchannels. We furthermore present a method to introduce pH changes into our modeling approach, which we employ in order to understand the conditions in the microchannels. The pH in turn depends on local concentration distributions of the components in the system. We take into account the pH gradient in the microchannel, which induces collagen gelation and correspondingly results in a dramatic increase in the collagen stream viscosity. Finally, we present X-ray microdiffraction experiments that suggest flow-induced subunit ordering of collagen fibrils.

Influence of the viscosity

Collagen is highly birefringent, a trait shared among many fibrous proteins. The signal is increased by (i) the alignment and assembly of many individual collagen molecules into liquid crystalline structures and (ii) anisotropic elongation and extension.[25]

In figure 2a a birefringence micrograph (lower half) of a hydrodynamically focused collagen stream is shown. The flow rate ratio is v_{main}:v_{side}=1:30, and the absolute flow rates are v_{main}=1.35 mm/s and v_{side}=40.5 mm/s. In this case, the collagen solution is diffusively mixed with its solvent (0.075 M AcH) flowing into the side inlet channels and therefore the pH in the system is constant in all channels. Thus, the collagen remains in its soluble form and no self-assembly occurs. Consequently, the observable birefringence signal is weak (red arrow), but the distinct shape (white dashed line, guide to the eye) of the viscous collagen stream in the center of the channels can be observed and deduced from the micrographs.

FEM simulations are very well suited to quantify the influence of viscosity effects and understand the hydrodynamics of the system. We use the FEMLAB® software applying about 10,000 finite elements. We first consider a system with spatially constant pH as is shown in figure 2a. In this case the viscosity in the center stream corresponds to the value for soluble collagen at a concentration of 10 mg/mL. In order to obtain a comparative value for solution viscosity, we use an Ubbelohde-viscometer to conduct bulk measurements ($\eta_{\text{collagen}} \sim 1800$ mPa·s). The bulk collagen viscosity is more than 2000 times higher than the viscosity of water η_{water}=0.891 mPa·s, which is the main component of the solvent (AcH). The result is particularly impressive when it is regarded that the volume fraction of collagen is merely $\phi \approx 0.01$. The FEM simulations include the Navier-Stokes equation and the diffusion equations for three inflowing streams where the center stream has a much higher viscosity than the side streams. The viscosity is fitted to $\eta_{\text{collagen}} = 2000$ $\eta_{\text{water}} = 1782$ mPa·s which is in good agreement with the result from viscometer measurements. In the simulations η_{collagen} is assumed to be proportional to the cube of c_{collagen}, thus slightly smoothing the transition in viscosity between the center and side streams. This approximation is used to accomplish better numerical handling of the system. The simulated viscosity in direct comparison to the experimental results is shown in figure 2a (upper half). Experiment and simulation agree well and the shape of the collagen stream along the interaction channel can be suitably fitted. The results demonstrate the consistency of bulk viscometry, microfluidics experiments, and FEM simulations. In turn, this ‘microchannel-rheology’ technique provides a method which enables us to evaluate the viscosity of minute quantities of very viscous fluids. Comparing the

experimental results and the simulated collagen stream (figure 2a) it is obvious that the experimental collagen stream is slightly curved into the aqueous stream at the confluence of the side and main inlets, a phenomenon which is not observed in this distinctness in the simulations. This is an effect of the finite height of the microchannels in the experiments (3D-case) in comparison to the simulations that were calculated for an infinite height (2D-case) as could be seen in simulations of a simplified system (data not shown). The additional no slip boundary condition on the top and bottom walls of the channel leads to a changed flow profile in proximity to the walls. It is important to note that the principal physical phenomena are still accurately described using the 2D scenario. However, computational complexity and coupled physical phenomena prohibited extensive 3D simulations.

Figure 2b shows the simulated flow field for the collagen system studied here ($\eta_{main} \gg \eta_{side}$.) The increased viscosity in the center stream leads to a dramatically increased flow rate of the side stream fluid at the confluence of all inflows, whereas the flow rate of the center stream itself remains almost constant. This is in striking contrast to a pure water/water system. In figure 2c, line scans along the center of the main channel parallel to the flow direction are shown. For a water/water system (dashed line, plotted for comparison) the flow is strongly accelerated in the center of the cross, where the inflows merge. Since all inflowing streams have the same viscosity, they behave like one single flow. This can also be observed in a line scan perpendicular to the main channel direction at x = 150 μm (figure 2d). Along the y-direction, the typical parabolic flow profile develops. Since $v_{\mathrm{main}} \ll v_{side}$, only a very small fraction of the main channel is occupied by the center stream, as indicated by the blue box in figure 2d. In contrast to this anticipated behavior, the collagen system is strikingly different. Owing to its high viscosity, the flow velocity of the center stream is not as influenced by the incoming side streams. Instead, the side streams are strongly accelerated. Consequently, the velocity profile parallel to the flow direction in the center of the main channel only very slowly increases and the acceleration region, where added biomolecules can be elongated, is extended into the main channel. Perpendicular to the flow direction we observe parabolic flow profiles developing in both side streams, whereas the flow velocity throughout the center stream remains constant in the lateral direction. The interfaces between the collagen solution and side streams act like additional ‘walls’ and the side streams flow as if in channels of smaller width. Eventually, the expected parabolic flow profile throughout the whole channel evolves. However, this occurs far downstream and is therefore not accounted for in our discussions. Fortunately, we can actually take advantage of the hydrodynamic conditions in the crossed channels. The slower but longer-lasting acceleration phase is used to align the collagen molecules in a more defined way.

Evolution of a pH gradient in the microchannels

The FEM simulations also provide detailed information about the concentration distribution of each reagent in the channels, as shown in figure 3a–c for a flow rate ratio of $v_{main} : v_{side}$ = 1:30 and c_{NaOH} = 0.075 M.

The simulated collagen distribution (a) yields a constant concentration (10 mg/mL) throughout the entire collagen stream and does not noticeably diffuse out of the center stream. This is due to the fact that the diffusion of collagen molecules in aqueous solution $D_{collagen} = 6.9 \cdot 10^{-12}$ m^2/s [26,27] is much slower than the diffusion of the relatively smaller OH^- ions and AcH molecules. The AcH (b) is more localized than the NaOH (c), which diffuses very fast into the center stream. We can understand these differences on the following two grounds. First of all, the diffusion constant of OH^- ($D_{OH^-} = 5.3 \cdot 10^{-9}$ m^2/s) is three times larger than of AcH ($D_{AcH} = 1.24 \cdot 10^{-9}$ m^2/s). Secondly, AcH diffuses out of the center stream and is flushed away by the suddenly increasing flow in the side streams before it has the opportunity to diffuse out further. Note that here we treat collagen and AcH solutions separately, since their diffusive

behavior differs even though they are injected into the main channel as a mixture. Solvent diffusion in semidilute polymer solutions can be described by the concept of obstruction effects. The existence of polymers in the solutions increases the path length of the diffusing molecules because they have to navigate through the polymer landscape. However, these effects are quite small and corresponding models[28,29] lead to effective diffusion constants which are merely 2 – 4 % smaller than the free diffusion constant. Corresponding concentration distributions can be determined for different flow rate ratios and give information about the local concentrations of NaOH and AcH, c_{NaOH} and c_{AcH}, at every position of the microfluidic device. These concentration profiles can be used to calculate the local pH distributions.

In the following paragraphs we will develop a method to calculate the pH as a function of the channel position in dependence of these concentration distributions.[30] In principle, a pH titration of a weak acid (AcH) with a strong base (NaOH) is conducted in the microfluidic device. However, the situation is more complicated since both the concentration of AcH and NaOH change constantly.

An analytical expression exists for a few specific points on a titration curve, such as for pure weak acid, for a pure strong base, and at the stoichiometric point, where the molarity of the weak acid and the strong base are equal. In order to find an analytical expression for the whole titration curve we determine the equations that define the problem and solve this system of equations.

It is necessary to perform a case differentiation and to set up a system of equations for the conditions before and after the stoichiometric point is reached, respectively. Before the stoichiometric point is reached we begin with a pure acid solution. The input AcH dissociates partially into acetate and hydronium ions and partially remains in the system as free AcH:

$$\mathrm{AcH} \leftrightarrow \mathrm{H^+ + Ac^-}$$

with

$$[\mathrm{AcH}] = [\mathrm{AcH}]_{free} + [\mathrm{Ac^-}] \tag{1}$$

where [AcH] is the local AcH concentration. Therefore we have to consider the definition of the acidity constant (for acetic acid in this example; however, all equations can be generalized for any weak acid and strong base)

$$K_s = \frac{[\mathrm{H^+}][\mathrm{Ac^-}]}{[\mathrm{AcH}]_{free}} = \frac{\alpha^2}{(1-\alpha)}[\mathrm{AcH}] = 1.78 \cdot 10^{-5} \tag{2}$$

where $[\mathrm{AcH}]_{free} = (1 - \alpha)[\mathrm{AcH}]$ and $[\mathrm{H^+}] = [\mathrm{Ac^-}] = \alpha[\mathrm{AcH}]$ with the degree of dissociation α.

Furthermore, we have to take into account the definition of the dissociation constant of water

$$K_W = [\mathrm{H^+}][\mathrm{OH^-}] = 10^{-14}. \tag{3}$$

Upon addition of NaOH these equilibrium conditions are affected. We need to ensure that the number of charges is conserved ($[Na^+] = [NaOH]$):

$$[H^+]+[Na^+]=[Ac^-]+[OH^-]. \tag{4}$$

Equations (1) – (4) have to be coupled and solved in order to determine the pH before the stoichiometric point is reached as a function of the acid and base concentrations.

After the stoichiometric point is reached, we must take into account that a sufficient amount of NaOH has now been added to the system in order to dissociate all input AcH (this is, in fact, the definition of the stoichiometric point). However, the resulting acetate ions react with water molecules, which in turn lead to additional formation of OH^- according to

$$H_2O+Ac^- \leftrightarrow OH^-+AcH.$$

Therefore, the effective OH^- concentration in the system is the input NaOH diminished by the OH^- which dissociates the input AcH and additionally the newly formed OH^-. This leads to the following relation:

$$[OH^-]=[AcH]_{free}+[NaOH] - [AcH]=[NaOH] - \alpha[AcH] \tag{5}$$

These equations need to be coupled and solved.

The equations can be solved analytically using Mathematica®. For $0 < [NaOH] < [AcH]$, that is, before the stoichiometric point is reached, we obtain the following solution:

$$\mathrm{pH}= - \log_{10}\left[\frac{\frac{1}{3}(-K_s - [NaOH])+2^{1/3}\xi}{3\left(\zeta+\sqrt{4\xi^3+\zeta}\right)^{1/3}} - \frac{1}{3\cdot 2^{1/3}}\left(\zeta+\sqrt{4\xi^3+\zeta}\right)^{1/3}\right], \tag{6}$$

where

$$\xi= - K_s^2 - 3K_s[AcH]+K_s[NaOH] - 3K_w - [NaOH]^2 \tag{7}$$

and

$$\zeta=2K_s^3 - 18K_sK_w+9K_s^2[AcH] - (3K_s^2 - 9K_w)[NaOH]+9K_s[AcH][NaOH] - 3K_s[NaOH]^2+2[NaOH]^3. \tag{8}$$

For $[NaOH] > [AcH]$, that is, after the stoichiometric point is reached, the solution is:

$$\mathrm{pH}= - \log_{10}\left[\frac{-\delta+\sqrt{4[NaOH]K_sK_w+\delta^2}}{2[NaOH]}\right] \tag{9}$$

where

$$\delta=([\mathrm{AcH}]-[\mathrm{NaOH}])K_s+K_w. \tag{10}$$

Both pH-equations (equations 6 and 9) only depend on two parameters, [AcH] and [NaOH], both of which are determined by the FEM simulations. The equations are implemented in a Matlab® program in order to calculate the pH at every specific position in the considered microfluidic device, resulting in a graphical representation of the pH distribution (see figure 4a–c).

Collagen gelation

If, in contrast to figure 2a, the AcH in the side inlets is replaced by a strongly basic solution of NaOH (0.075 – 0.5 M), a stable pH gradient is established in the outlet channel. The collagen begins to self-assemble, and we observe a stronger birefringence signal at the edges of the collagen stream (figure 3d). Therefore the regions within the stream where the collagen is assembled can be identified by an increase of the birefringence signal. In addition to the increase of the birefringence signal upon self-assembly of the collagen molecules, a clear change in shape of the collagen stream can be observed (figure 3e). This indicates a further increase in viscosity. Indeed, bulk experiments have shown that the viscosity of a collagen solution is dramatically increased once the pH is increased and the collagen gelation process advances.[31] In the microdevices used here, as the pH increases - and the collagen self-assembly consequently proceeds - the shape of the focused collagen stream in the crossed channel device changes. Namely, it becomes more extended into the outlet channel. To characterize the collagen assembly, we consider the system where the pH gradually changes within the microchannel in the modeling approach. We aim to numerically describe the following situation: NaOH diffuses into the center stream, which changes the pH of the collagen solution and induces a gelation of the collagen which, in turn, leads to an increase of the viscosity. Therefore, we have to couple the viscosity to the local pH of the system which is itself a function of the solvent concentrations c_{NaOH} and c_{AcH}. The functional dependence of the viscosity on the pH and thus on the acid and base concentrations has to be described by a single function. The situation can be well approximated by

$$\eta \approx \eta_{collagen}+\eta_{gel} \tag{11}$$

with

$$\eta_{gel}=r_1 c_{collagen}{}^3(\tanh(r_2([\mathrm{NaOH}]-[\mathrm{AcH}]-f_{gel}^{\mathrm{pH}}([\mathrm{NaOH}],[\mathrm{AcH}])))+1) \tag{12}$$

with two fit parameters r_1 and r_2. The numerical value of r_1 determines the maximum viscosity of the assembled collagen and r_2 determines the shape of the function. $\eta_{collagen}$ = 1782 mPa·s is known from the control experiment without collagen assembly. The function $f_{gel}^{\mathrm{pH}}([\mathrm{NaOH}],[\mathrm{AcH}])$ describes the deviation of the point of inflection/threshold value from the stoichiometric point; where the concentrations of AcH and NaOH are equal.

Calculating the pH distribution in the crossed channels yields the possibility to directly compare experiment and simulation and thus determine how collagen gelation is related to the local pH. In figure 4, birefringence micrographs of the collagen assembly process at three different flow rate ratios are shown. The respective concentration distributions of AcH and NaOH together with equations describing the local pH in dependence of these concentrations are used to

calculate the complete pH conditions for every position in the microchannels. Since the reaction kinetics are faster than the diffusion, we assume that gelation takes place immediately after the solutions are mixed and the pH has reached a certain threshold value. The shape of the birefringence signal and the shape of the simulated pH distribution correspond well for all three flow rate ratios. We obtain good results for r_1 = 245 Pa·s, r_2 = 100 and a chosen $f_{gel}^{\mathrm{pH}}([\mathrm{NaOH}],[\mathrm{AcH}]) \approx 0$, which corresponds to an onset/threshold of the gelation at an almost neutral pH, in equation 12. The viscosity of the assembled collagen η_{gel} (equation 12) is extremely high, five orders of magnitude higher than η_{water} and two orders of magnitude higher than $\eta_{collagen}$. These results agree remarkably well with bulk experiments. For gelled collagen solutions with $c_{collagen}$ = 3 – 5 mg/mL a viscosity of η_{gel} ~ 140 Pa·s has been determined.[31] Our results are on the same order of magnitude and slightly higher due to the higher collagen concentration. The strong increase in birefringence intensity, which is due to the gelation and consequently lateral arrangement of collagen molecules in flow, can be observed in the regions where ~ pH 6 – 8 (green). Interestingly, these pH values have been associated with the onset of the assembly of collagen I for bulk experiments.[32] This result shows that our experimental findings as well as the numerical description are consistent. The birefringence micrographs as well as the simulated data are further compared by analyzing line scans at specific positions in the channel (figure 4d–f). For each line scan of the birefringence intensity, the signal is averaged over 15 images and 20 lines in each image and the resulting intensity is normalized. The points of maximum intensity correspond to the borders of the flow where the collagen is already assembled. In figure 4b three different positions (x = 50, 100, 200 μm) in the crossed channels are marked by colored lines. The corresponding line scans for a fixed flow rate ratio v_{main}: v_{side}= 3 : 30 are shown in figure 4d. The solid lines show the birefringence intensity data and the dashed lines the corresponding course of the pH distribution. Each pair of curves intersects at approximately pH 7 which supports our observation that the gelation occurs at almost neutral pH. In figure 4e we compare line scans at the same position x =100 μm in the channel for different flow rate ratios. Again, the solid lines show the birefringence intensity whereas the dashed lines show the corresponding pH distribution. In this case we observe a better agreement of experiment and simulation for slower side stream velocities. In figure 4f line scans of the pH distribution along the main channel direction in the center of the channel are shown. The pH does not increase to neutral in the considered region and, as expected in the light of this fact, we do not observe a strong increase of the birefringence intensity along the main channel. Altogether we find that the experimental system can be well described by the FEM simulations and the determination of the pH distribution in the channels is well suited to understand the processes of fibril formation. The diffusive mixing of NaOH and acidic collagen solution leads to a stable pH gradient, which in turn induces self-assembly of the collagen molecules starting at a pH of ~ 6 – 8. The self-assembly can directly be visualized by an increase in birefringence signal and coincides with a dramatic increase in solution viscosity from ~ 2 Pa·s up to ~ 500 Pa·s. At the same time, we are able to model the conditions in the microchannels, allowing us to semi-quantitatively determine the interdependence of viscosity, pH distribution, and flow profiles. Our results, which are validated by corresponding bulk measurements, show that the technique is indeed suitable to investigate reactive non-equilibrium systems on the microscale. In particular, the numerical descriptions developed here can extend more generally to any strong base – weak acid system.

Molecular ordering quantified using X-ray microdiffraction

In the previous sections we have presented results of polarized light microscopy experiments and FEM simulations that established the study of collagen self-assembly and characterization of the system on a micrometer scale. However, it is also highly desirable to study the system on a molecular length scale. At the same time, it is our aim to investigate the dynamics of fibril formation. Therefore, X-ray microdiffraction in combination with microfluidics is an excellent tool for our purposes. A unique feature of our setup is that the steady, continuous flow enables

in situ investigation of the pH-induced collagen assembly without material damage. Using with a microfocused X-ray beam, we are particularly well-equipped to investigate the molecular packing and ordering of collagen molecules at different positions in the channels with high resolution. We conduct appropriate FEM simulations in order to relate the measured X-ray signal to the hydrodynamic, diffusive, and pH related phenomena in the channel. In figure 5a the simulated viscosity (upper half of the image) and pH distribution (lower half) are shown. The flow rate ratio is v_{main}:v_{side}==1:2.4 and the absolute flow rates are v_{main} = 1050 μm/s and v_{side} = 2520 μm/s. The input collagen concentration is 10 mg/mL in 0.075 M AcH and the NaOH concentration is c_{NaOH} = 0.5 M. Compared to the parameters used for the birefringence experiments, a much larger fraction of the center stream contains assembled collagen and is therefore highly viscous. We collect X-ray diffraction scattering patterns at different positions perpendicular to the main channel, as noted in figure 5a by circles. The corresponding intensities are plotted against the reciprocal space *q*-vector in figure 5b. Intensity plots are obtained by a radial integration of the two-dimensional diffraction images, an example of which is shown in figure 5c. A distinct correlation peak at $q = 1.46\ \mathrm{nm}^{-1}$, which corresponds to a spacing of $d = 2\pi/q = 4.3$ nm, is observed in the center of the cross and is even more pronounced at y = 30 μm. Thus, a supramolecular structure can be found in the system yielding a characteristic length scale of d = 4.3 nm. In the side channel, at y = 120 μm, there is no collagen present and consequently no observable peak. A weak maximum of the azimuthal distribution at $q = 1.46\ \mathrm{nm}^{-1}$ with $\chi_{\max} \approx 67°$ and $\chi_{\max} \approx 247°$, where $\chi = 0°,180°$ correspond to a perpendicular orientation to the main channel and $\chi = 90°, 270°$ correspond to a parallel orientation to the main channel, is observed (figure 5d). These maxima can be attributed to a preferred orientation of the collagen fibrils along the streamlines of the collagen jet (figure 5a).

Somewhat counterintuitively, we do not observe the most intense X-ray peak in the regions where we detect the brightest birefringence signal in corresponding polarized light microscopy experiments. That is to say, in those positions where the viscosity of the collagen solution is strongly increased due to self-assembly at ~ pH 6–8, the X-ray peak is not correspondingly intense. In contrast, the strongest X-ray peak is detected close to the center region. However, X-ray measurements on *in vivo* systems such as rat tail tendon[33] or cornea[4] have revealed a diameter for the subunits that form from the collagen molecules of around 4 nm, which is in agreement with our result. Moreover, the characteristic spacing of ~ 4 nm is consistent with the model for the packing of type I collagen molecules in the native fibril that was suggested by Piez and Trus in 1981.[34] One reasonable interpretation of our X-ray data is the following: in the center region of the cross the pH conditions ~ 4 – 5 lead to the formation of pentameric subunits, which subsequently transitions to a dense packing of collagen monomers in regions of optimal pH ~ 6 – 8. It is important to note that some bulk experiments[35,36] and theoretical studies[34,37] have shown that upon further lateral compression, previously formed pentameric subunits disappear and a near-hexagonal lattice of the molecules forms. Additionally, it is clear from the experiments with polarized microscopy that a strong birefringence signal is correlated with highly viscous collagen solution which, in turn, indicates that the molecules are assembled in larger aggregates. We propose that in the highly birefringent regions, the previously reported quasi-hexagonal phase of collagen molecules has already formed. The *q*-range of our setup at the synchrotron is 0.2 – 2.5 nm^{-1}, corresponding to d = 2.5 – 31.4 nm. Since the spacing of the close packed hexagonal phase is similar to the diameter of the collagen molecules (~ 1.5 nm), we cannot observe a corresponding signal in the experiments. However, we do see an indisputable decrease in X-ray signal from the feature at ~ 4 nm, which would be expected during such a transition from a pentameric to close packed organization.

In order to gain more insight into the origin of the peak $q = 1.46\ \mathrm{nm}^{-1}$ seen in microflow, ‘bulk experiments’ in capillaries were also conducted. Aqueous solutions of collagen ($c_{collagen}$ = 5 mg/mL) at pH 5, 8, and 11 were measured using an in-house small angle scattering setup. The scattering from these samples (figure 6) shows no evidence of a feature on the same length

scale as that measured in flow, regardless of the sample solution pH. However, an increase in the small angle intensity is observed for samples with pH ≥ 7, which is characteristic of scattering from a gel solution. In wide angle measurements, a peak at $q = 6\ nm^{-1}$ ($d = 1.0$ nm) can be observed after drying the collagen sample, which cannot be observed in the aqueous solution (figure 6, inset, pH 11). This spacing is consistent with an interpretation of a close hexagonal packing of collagen molecules, since it is on the order of the diameter of single collagen molecules. The fact that in these bulk experiments we only find a supramolecular structure upon drying of the sample supports the interpretation that in the fluid state the intrinsic disorder of the macromolecules (as prepared in capillaries) prevents us from detecting a characteristic length scale in the system. Furthermore, at no point do we measure a peak corresponding to 4.3 nm, such as that seen in the microfluidic experiment. This suggests that we create unique microenvironments by aligning the collagen fibrils in a well-defined pH gradient, resulting in a highly controlled mixing scenario that is not reproduced by bulk experiments. In the microflow devices, we impose external forces on the system that enable the assembly to proceed into distinct structures – even in solutions. With the appropriate selection of observation points in the pH gradient, we are able to perform non-equilibrium measurements of different stages of fibril formation, all using only one single device. As is evidenced by the apparent discrepancy between X-ray measurement in flow or in bulk, the tunability of experimental conditions via adjustment of concentrations and flow rates within our well described diffusion-based mixing environment results in an incomparable approach to the systematic study of reactive biological systems.

Conclusions

The combination of FEM simulations, microfluidics, microscopy, and X-ray microdiffraction provides a particularly well suited method to investigate biological systems, as we show here for the example of collagen. It proves to be crucial to relate hydrodynamic phenomena in the microfluidic channel to the occurring self-assembly processes. Taking into account the increasing viscosity of collagen upon onset of gelation we are able to thoroughly describe the system. In this context we determine the supramolecular structure of the forming collagen fibril on the micro- and the nanoscale.

We develop analytical expressions in order to calculate the gradient of pH formed in flow, and compare this directly with cross polarized microscopy. In this case, the formation of fibrils occurs precisely in regions of pH ~ 7 where the viscosity also increases many-fold. Somewhat less intuitively, X-ray microdiffraction experiments in flow reveal a supramolecular assembly of collagen with a spacing of 4.3 nm, but this is primarily found in regions of the device where the pH is between 4 and 5. This is where we observe the strongest signal. The peak intensity decays in regions where the solution is most viscous, with pH ~ 7. The spacing of this feature is consistent with a pentameric assembly of collagen, and it is not reproduced in separate collagen bulk solution experiments, indicating that the setup in flow accesses distinct well-mixed experimental conditions. The results are in agreement with bulk measurements, *in vivo* studies, and existing theoretical models and add an important component to the completion of the picture of hierarchical collagen self-assembly.

The approach that we demonstrate here suggests many other uses for researchers interested in the creation of unambiguous chemical environments, with predictable solution mixing that allow simultaneous experimental observation. In principle, the pH model presented here is sufficient for any strong base-weak acid interaction. Furthermore, an online pH titration is also feasible with the appropriate choice of measurement position along fixed stream lines. It is possible to characterize material properties, such as the viscosity of an assembly and its supramolecular organization, using the approach outlined in this work. The creation of aligned

materials, in particular those such as collagen that are biologically active, opens new research directions for cell-protein interactions and other complex biomaterial phenomena.

Acknowledgements

We thank the National Science Foundation and German Science Foundation (DFG) (German-American Frontiers in Polymer Science) for initiating the collaboration. We thank Stephan Herminghaus, Dagmar Steinhauser, Jennie B. Leach, Oleg Konovalov, and Bernd Struth for fruitful discussions and Udo Krafft for his excellent technical assistance. We acknowledge the European Synchrotron Radiation Facility (ESRF). This work was supported by the Emmy-Noether-Program of the DFG (PF 375/2-3). H.M.E. acknowledges a fellowship from the Alexander von Humboldt Foundation. J.Y.W. acknowledges support from NIH NHLBI.

References

1. Thakar RG, Ho F, Huang NF, Liepmann D, Li S. Biochem Biophys Res Commun 2003;307:883–890. [PubMed: 12878194]
2. Hodge, AJ.; Petruska, JA. Aspects of Protein Chemistry. Ramachandran, GN., editor. Academic Press; London: 1963. p. 289-300.
3. Orgel JPRO, Miller A, Irving TC, Fischetti RF, Hammersley AP, Wess TJ. Structure 2001;9:1061–1069. [PubMed: 11709170]
4. Holmes DF, Gilpin CJ, Baldock C, Ziese U, Koster AJ, Kadler KE. Proc Natl Acad Sci USA 2001;98:7307–7312. [PubMed: 11390960]
5. Miller A, Wray JS. Nature 1971;230:437–439. [PubMed: 4929973]
6. Christiansen DL, Huang EK, Silver FH. Matrix Biol 2000;19:409–420. [PubMed: 10980417]
7. Fung, YC. Biomechanics: Mechanical Properties of Living Tissues. Springer; New York: 1993.
8. Haga H, Irahara C, Kobayashi R, Nakagaki T, Kawabata K. Biophys J 2005;88:2250–2256. [PubMed: 15596493]
9. Murthy NS. Biopolymers 1984;23:1261–1267. [PubMed: 6466766]
10. Guido S, Tranquillo RT. J Cell Sci 1993;105:317–331. [PubMed: 8408268]
11. Jiang F, Horber H, Howard J, Muller DJ. J Struct Biol 2004;148:268–278. [PubMed: 15522775]
12. Wilson DL, Martin R, Hong S, Cronin-Golomb M, Mirkin CA, Kaplan DL. Proc Natl Acad Sci USA 2001;98:13660–13664. [PubMed: 11707577]
13. Köster S, Leach JB, Struth B, Pfohl T, Wong JY. Langmuir 2007;23:357–359. [PubMed: 17209575]
14. Pfohl T, Otten A, Köster S, Dootz R, Struth B, Evans HM. Biomacromolecules 2007;8:2167–2172. [PubMed: 17579478]
15. Dootz R, Evans HM, Köster S, Pfohl T. Small 2007;3:96–100. [PubMed: 17294477]
16. McPherson JM, Wallace DG, Sawamura SJ, Conti A, Condell RA, Wade S, Piez KA. Coll Relat Res 1985;5:119–135. [PubMed: 3924470]
17. Delamarche E, Bernard A, Schmid H, Bietsch A, Michel B, Biebuyck H. J Am Chem Soc 1998;120:500–508.Xia Y, Whitesides G. Ann Rev Mat Sci 1998;28:153–184.
18. Köster S, Steinhauser D, Pfohl T. Journal of Physics: Condensed Matter 2005;17:S4091–4104.
19. Knight JB, Vishwanath A, Brody JP, Austin RH. Phys Rev Lett 1998;80:3863–3866.
20. Otten A, Köster S, Struth B, Snigirev A, Pfohl T. J Synchrotron Rad 2005;12:745–750.Pfohl T, Mugele F, Seemann R, Herminghaus S. ChemPhysChem 2003;4:1291–1298. [PubMed: 14714376]
21. Cabrera CR, Finlayson B, Yager P. Anal Chem 2001;73:658–666. [PubMed: 11217778]Munson M, Yager P. Anal Chim Acta 2004;507:63–71.
22. Struth B, Snigirev A, Konovalov O, Otten A, Gauggel R, Pfohl T. AIP Conferenence Proceceedings 2004;705:804–807.
23. Snigirev A, Kohn V, Snigireva I, Lengeler B. Nature 1996;384:49–51.
24. Lengeler B, Schroer C, Benner B, Gerhardus A, Gunzler T, Kuhlmann M, Meyer J, Zimprich C. J Synchrotron Rad 2002;9:119–124.
25. Junqueira, LC.; Carneiro, J. Histologie. Springer; Heidelberg: 1996. p. 151
26. Atkins, PW. Physical Chemistry. Oxford University Press; 1998. p. 946-948.

27. For numerical reasons, we consider a diffusion constant which is higher $D_{simulation} \sim 5 \cdot 10^{-11}$ m^2/s, which reflects the real conditions quite well, since even this diffusion constant is two orders of magnitude smaller than the other relevant diffusion constants D_{OH^-} and D_{AcH}.
28. Mackie JS, Meares P. P Roy Soc Lon A 1955;232:498–509.
29. Waggoner RA, Blum FD, MacElroy JMD. Macromolecules 1993;26:6841–6848.
30. Köster S, Leach JB, Wong JY, Pfohl T. Mater Res Soc Symp Proc 2006;898E:0898-L05–21.
31. Newman S, Cloitre M, Allain C, Forgacs G, Beysens D. Biopolymers 1997;41:337–347. [PubMed: 10917694]
32. Cassel JM, Mandlekern L, Roberts DE. J Am Leather Chemists Assn 1962;57:556–575.
33. Miller A, Wray JS. Nature 1971;230:437–439. [PubMed: 4929973]
34. Piez KA, Trus BL. Biosci Rep 1981;1:801–810. [PubMed: 7306686]
35. Miller A, Tocchetti D. Int J Biol Macromol 1981;3:9–18.
36. Fraser RDB, McRae TP. Int J Biol Macromol 1981;3:193–200.
37. Wess TJ, Hammersley AP, Wess L, Miller A. J Struct Biol 1998;122:92–100. [PubMed: 9724609]

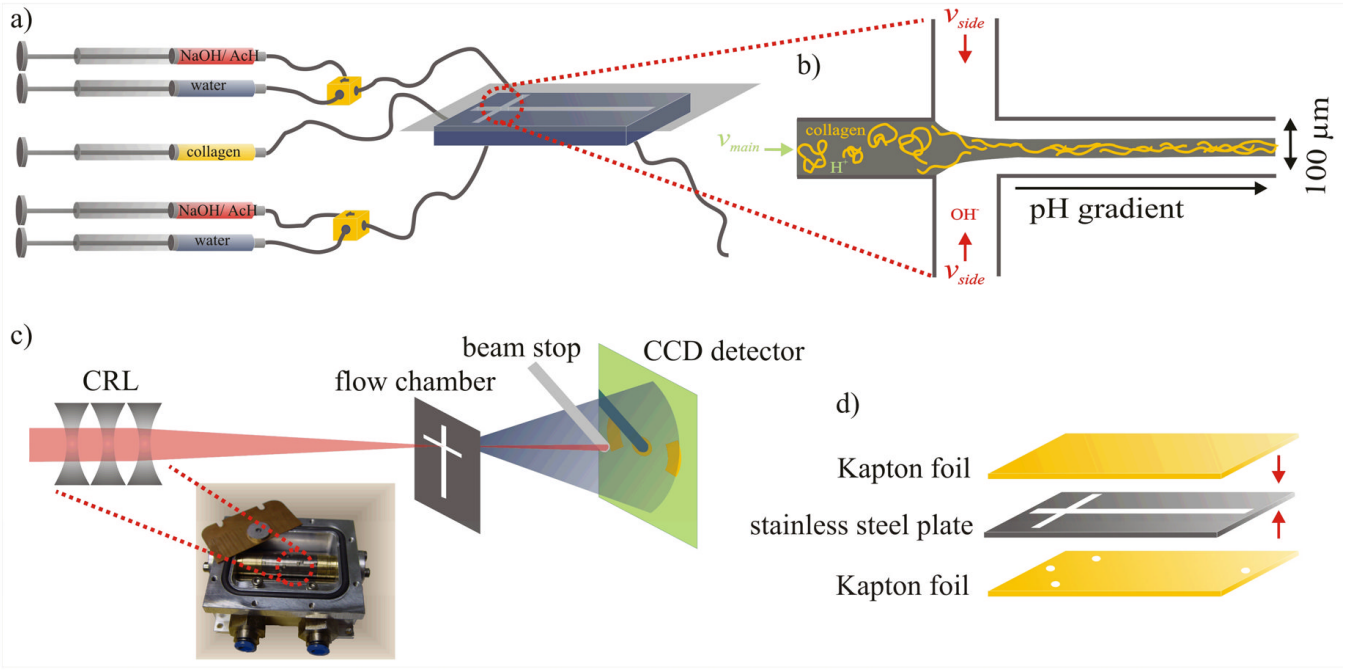

Figure 1.

Schematic of the experimental setup. a) Microsyringes are connected via tubing to the PDMS-microfluidic device. b) Top view of the flow channel geometry. The acidic collagen solution is injected into the center channels while the NaOH-solution in injected into the side channels. A pH gradient develops after the intersection of all channels. c) X-ray microdiffraction setup consisting of compound refractive lenses (CRL), the flow chamber, and a CCD detector. d) Design of the flow chambers used for X-ray diffraction experiments.

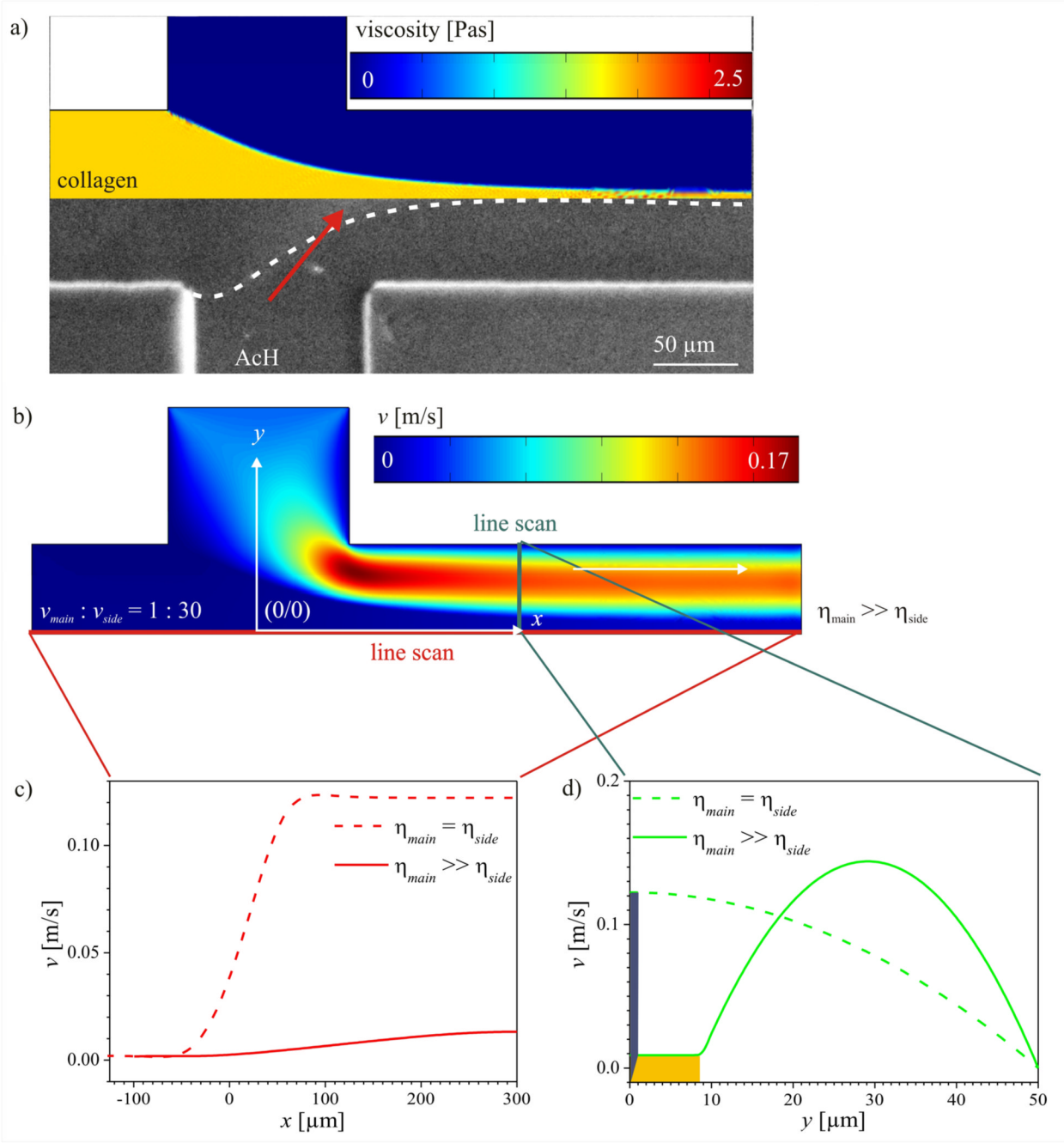

Figure 2.

Fitting solution viscosities to stream shape and flow profiles. a) Measured (bottom) and simulated (top) shape of a stream of viscous fluid hydrodynamically focused by aqueous solution. Red arrow: increased birefringence signal owing to highly aligned collagen molecules. b) Simulated velocity field for high viscosity center stream. c) Line scans along the center channel. Solid line: Viscous fluid in center channel, water in side channels; dashed line: water/water system for comparison. d) Line scans perpendicular to the center channel. The yellow box shows the fraction of the channel which is occupied by the viscous fluid in the center channel. The dark blue box shows the fraction of the channel which is occupied by the center stream for the water/water system.

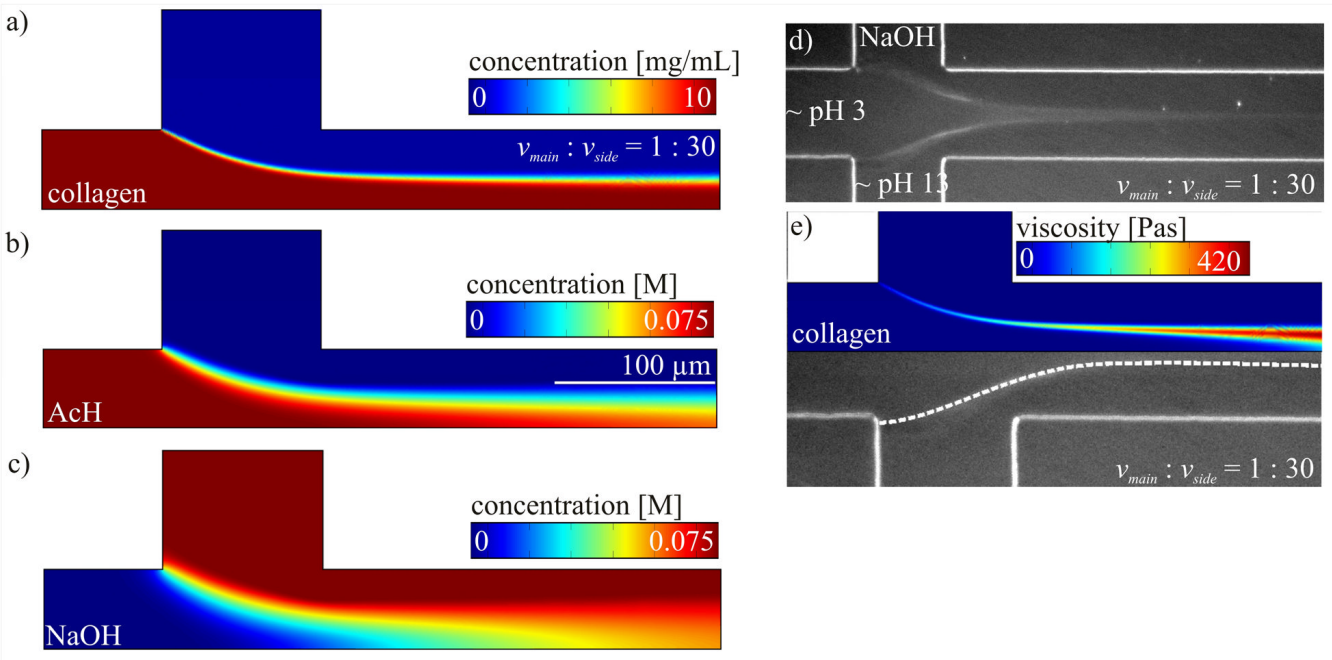

Figure 3.

a–c) Concentration distributions for collagen, acetic acid and sodium hydroxide, respectively. d) Influence of collagen gelation in a pH gradient on stream shape.e) Comparison of experimental result (bottom, birefringence signal) and simulation (top, viscosity).

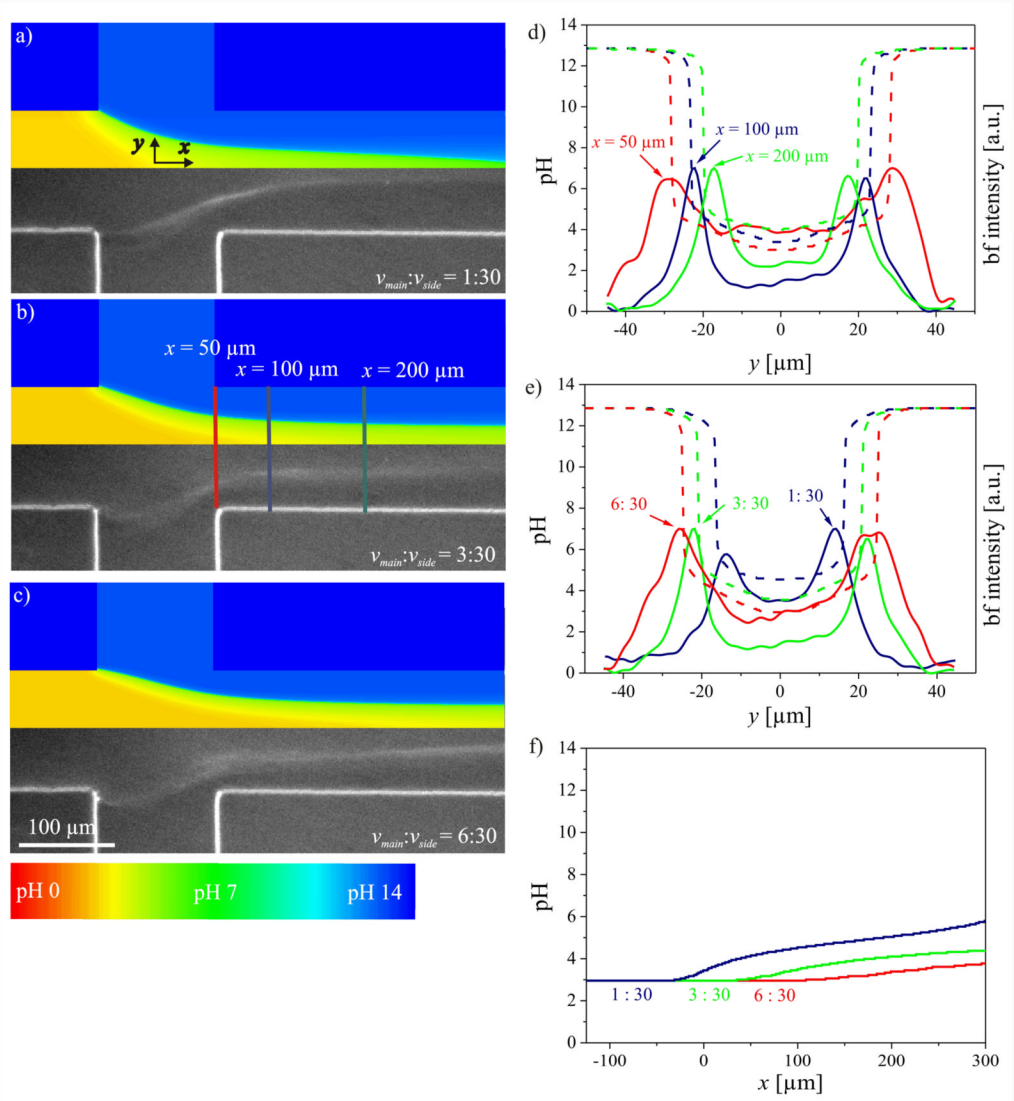

Figure 4.

Collagen gelation in pH gradient: Comparison of experiment and simulation. a–c) Simulations (top) and experimental results (bottom) for different flow rate ratios. d) Line scans at different positions for flow rate ratio v_{main}:v_{side} = 3:30. e) Line scans at x = 100 fm for different flow rate ratios. f) Line scans for y = 0 fm for different flow rate ratios.

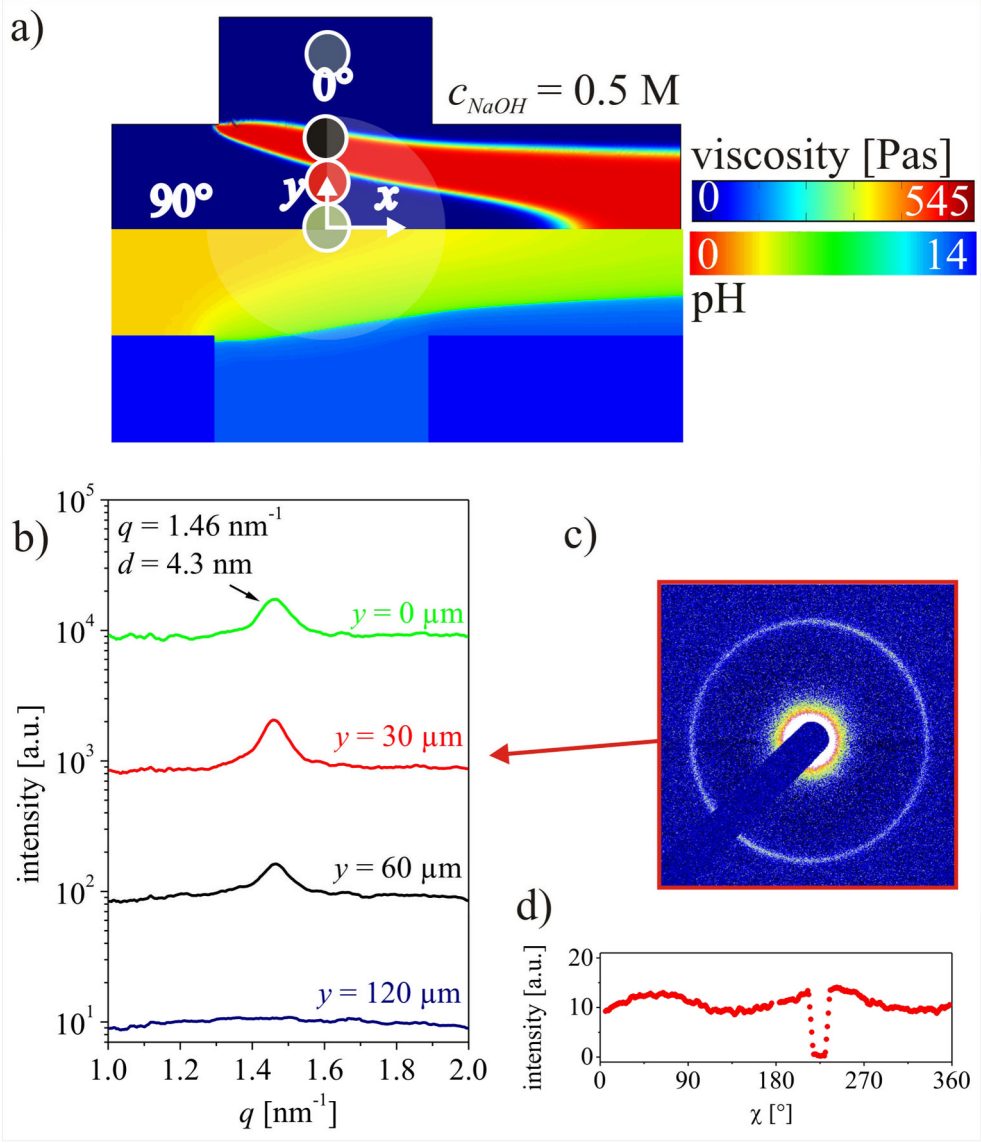

Figure 5.

X-ray microdiffraction. a) Top: simulated viscosity, bottom simulated pH. Colored circles denote the positions where data have been taken. b) X-ray diffraction scans as obtained from radial integration of scattering data. c) 2D-Scattering image taken at position y = 30fm. d) The azimuthal intensity distribution of the peak shows a weak orientation.

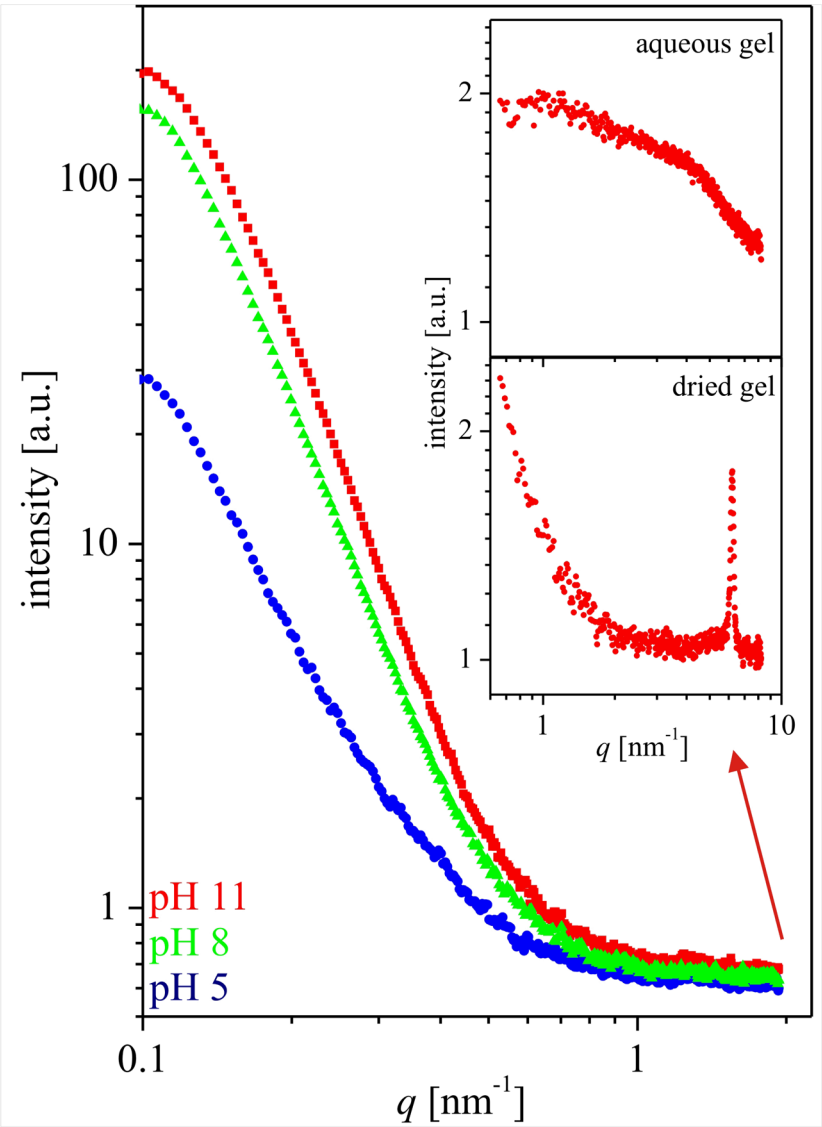

Figure 6.
Aqueous collagen samples at pH 5, 8, and 11 show no small angle scattering peak, compared to the peak observed at wide angle for a dried sample (inset, pH 11).